Di-Ureasil Hybrids Doped with $LiBF_4$: Attractive Candidates as Electrolytes for "Smart Windows"

Paula C. Barbosa[1], Mariana Fernandes[2], Sérgio M. F. Vilela[2,3], A. Gonçalves[4], M. C. Oliveira[2], E. Fortunato[4], M. Manuela Silva[1], Michael J. Smith[1], R. Rego[2], Verónica de Zea Bermudez[2,]*

[1] Departamento de Química/Centro de Química, Universidade do Minho, Campus de Gualtar, 4710-057 Braga, Portugal
[2] Departamento de Química /CQ-VR, Universidade de Trás-os-Montes e Alto Douro, 5001-801 Vila Real, Portugal
[3] Departamento de Química/ CICECO, Universidade de Aveiro, 3810-193 Aveiro, Portugal
[4] CENIMAT/I3N, Departamento de Ciência dos Materiais, Faculdade de Ciências e Tecnologia, FCT Universidade Nova de Lisboa, 2829-516 Caparica, Portugal
[*]E-mail: vbermude@utad.pt

Received: 1 November 2011 / *Accepted:* 1 December 2011 / *Published:* 1 January 2011

The sol-gel process has been used to prepare hybrid electrolytes composed of a poly(oxyethylene) (POE)/siloxane hybrid network doped with lithium tetrafluoroborate ($LiBF_4$) with compositions of n between ∞ and 2.5. In this context the lithium salt concentration is expressed in terms of the number of oxyethylene units in the organic component of the network per Li^+ ion. Electrolyte samples with $n \geq 20$ are thermally stable up to approximately 250 ºC. All the materials synthesized are semi-crystalline: in the composition range $n \geq 15$ free crystalline POE exists and at $60 \geq n \geq 2.5$ evidence of the presence of a crystalline POE/$LiBF_4$ compound has been found. At n = 2.5 this latter crystalline phase coexists with free salt. The room temperature conductivity maximum of this electrolyte system is located at n = 10 (1.5×10^{-5} S cm^{-1} at 22 ºC). The electrochemical stability domain of the sample with n = 15 spans about 5.5 V *versus* Li/Li^+. This new series of materials represents a promising alternative to the $LiTFSI^-$ and $LiClO_4$-doped POE and POE/siloxane analogues. Preliminary tests performed with a prototype electrochromic device (ECD) comprising the sample with n = 8 as electrolyte and WO_3 as cathodically coloring layer are extremely encouraging. The device exhibits switching time around 50 s, an optical density change of 0.13, open circuit memory of about 4 months and high coloration efficiency (106 cm^2C^{-1} in the 3rd cycle).

Keywords: organic/inorganic hybrid electrolytes, lithium trifluoroborate, ionic conductivity, cyclic voltammetry, electrochromic device

1. INTRODUCTION

Polymer electrolytes (PE) are complexes formed between ionic salts and polymers with electron-donor atoms, such as linear high molecular weight poly(oxyethylene) (POE). These materials are in general divided into two groups: solid (or solvent-free) PEs (designated as SPEs) and gel polymer electrolytes [1].

SPEs were first introduced by Armand et al. [2] as an attractive alternative to non-aqueous liquid electrolytes in light-weight, rechargeable lithium m batteries. The advantages of these materials include good electrochemical properties, a reduction in problems related to safety and environmental issues, and elimination of electrolyte leakage problems. These electrolytes may assume a multifunctional role as separator, adhesive and cell sealant in electrochemical devices. Li^+-based SPEs are considered to be attractive materials for application in electrochemical devices such as galvanic cells, electrochromic displays and sensors [3].

In spite of their technological potential, SPEs suffer from a series of drawbacks that have delayed their application in commercial devices. These include a marked tendency to crystallize, substantially lower ionic conductivity (typically 10^{-8} to 10^{-5} Scm^{-1} at room temperature) than non-aqueous liquid electrolytes and a tendency for the ionic guest species to salt out at high salt concentration. As liquid electrolytes also pose significant safety and environmental concerns, in recent years considerable effort have been devoted to increasing the ionic conductivity and improving the mechanical properties of SPEs [1].

One of the most successful strategies that have been applied in the development of improved SPEs is based on the exploitation of the organic/inorganic hybrid concept [4]. This approach makes use of the versatile and simple sol-gel method [5] and the resulting POE/siloxane hybrid host frameworks represent a class of essentially amorphous modified SPEs or ormolytes (organically modified silicate electrolyte). In general these materials exhibit good film-forming properties and high thermal, mechanical and chemical stability. In addition they have the ability of accommodating considerably higher guest salt concentrations than conventional SPEs without any undesirable consequences. Several Li^+-doped ormolytes emerged from the sustained research carried out in this domain [6-20]. We have been particularly interested in the application of the di-urea cross-linked POE/siloxane hybrid frameworks in this context [14-19]. These hybrid structures, designated as di-ureasils [21] have been represented as d-U(Y), where d indicates di, U denotes the urea (-NHC(=O)NH-) group and Y = 2000, 900 and 600 represents the average molecular weight of the starting organic precursor, corresponding to 40.5, 15.5 and 8.5 $-CH_2CH_2O-$ repeat units.

The encouraging conductivity values displayed by ormolytes composed of the d-(900)- and d-U(600)-based di-ureasils and lithium tetrafluoroborate ($LiBF_4$) [22] and by ormolytes incorporating the d-U(2000) matrix and lithium triflate ($LiCF_3SO_3$) [14], lithium perchlorate ($LiClO_4$) [16] and lithium bis(trifluoromethanesulfonyl)imide (LiTFSI) [18] have led us to investigate in the present work d-U(2000)-based ormolytes doped with $LiBF_4$.

Several recent papers by Zhang et al. [23-25] have demonstrated that $LiBF_4$-based electrolytes are a good alternative to lithium hexafluorophosphate ($LiPF_6$)-based materials as components in low temperature Li-ion batteries with improved performance. These authors found that, although an electrolyte based on a solution of $LiBF_4$ in propylene carbonate/ethylene carbonate/ethylmethyl carbonate had lower ionic conductivity and a higher freezing temperature than the $LiPF_6$-based analogue, at –20 ºC the $LiBF_4$–based cell had lower charge-transfer resistance than the $LiPF_6$–based device. In spite of the slightly lower conductivity of the $LiBF_4$-based electrolyte, the cell based on this system showed slightly lower polarization and higher capacity in the liquid temperature range (above –20 ºC) of the electrolyte. These results suggested that the ionic conductivity of the electrolytes is not

necessarily a limitation to the low-temperature performance of the Li-ion cell. The $LiBF_4$ salt may be a good choice for a low temperature electrolyte of a Li-ion cell if a solvent system that has low freezing temperature, high solubility towards $LiBF_4$, and good compatibility with a graphite anode can be formulated. Examples of SPEs doped with $LiBF_4$ and supporting acceptable levels of room temperature ionic conductivity have already been reported [22,26-29].

The present work has been focused on a d-U(2000)-based di-ureasil system containing a wide range of $LiBF_4$ concentrations. A vibrational spectroscopic analysis of the extent and magnitude of ionic association and hydrogen bonding interactions in this set of di-ureasil samples have been reported very recently [30]. Here, the structure, morphology, thermal stability, ionic conductivity and electrochemical stability of this series of materials have been characterized. Exploratory studies of the performance of prototype ECDs in which optimized compositions of the $LiBF_4$-doped di-ureasils have been used as ion conducting active layers have been also carried out.

2. EXPERIMENTAL

2.1. Materials

Lithium tetrafluoroborate ($LiBF_4$, Aldrich, 99.998%) and O,O'-bis-(2-aminopropyl) polypropylene glycol-block-polyethylene glycol-block polypropylene glycol (Jeffamine ED-2001®, Fluka, average molecular weight MW ≈ 2001 $gmol^{-1}$ (Scheme 1) were dried under vacuum at 25 ºC for several days prior to being used. The bridging agent, 3-isocyanatepropyltriethoxysilane (ICPTES, Aldrich 95%), was used as received. Ethanol (CH_3CH_2OH, Merck, 99.8%) and tetrahydrofuran (THF, Merck, 99.9%) were dried over molecular sieves. High purity distilled water was used in all experiments.

2.2. Preparation of the ormolytes

The synthetic procedure used to prepare the $LiBF_4$ -based di-ureasils has been described in detail elsewhere [14,16,18]. It involved grafting the Jeffamine2001® diamine onto the ICPTES precursor to yield the di-urea (-NH(C=O)NH-) bridged hybrid molecule. This precursor was subsequently hydrolyzed and condensed in the sol-gel stage of ormolyte preparation to induce the growth of the siloxane network. In agreement with the terminology adopted in previous publications [14-19], the ormolytes were identified using the notation d-U(2000)$_n$$LiBF_4$ (where n represents the molar ratio of oxyethylene units per Li^+ ion) and samples were prepared with n = ∞, 200, 80, 60, 40, 30, 20, 15, 10, 8, 5 and 2.5.

2.3. Characterization of the ormolytes

Sections of the ormolytes for Differential Scanning Calorimetry (DSC) characterization were removed from dry films and subjected to thermal analysis under a flowing argon atmosphere between

25 and 300 ºC and at a heating rate of 5 ºC.min^{-1} using a Mettler DSC 821e. These samples were transferred to 40 µL aluminium cans with perforated lids within a dry argon-filled glovebox.

Samples for thermogravimetric analysis (TGA) were prepared in a similar manner, transferred to open crucibles and analyzed using a Rheometric Scientific TG1000 thermobalance operating under flowing argon.

Polarized Optical Microscopy (POM) images were recorded using an OPTIKA B-600POL microscope equipped with a 8M pixel Digital Photo Camera. The images were analyzed using with the OPTIKA VISION PRO software.

X-ray diffraction (XRD) patterns of di-ureasil samples were recorded at room temperature with a PANalytical X'Pert Pro diffractometer equipped with a X'Celerator PW3015/20 detector using monochromated CuK_α radiation (λ = 1.54 Å) between 5 and 80º (2θ). Owing to the poor mechanical properties of the salt-rich samples with n = 5 and 2.5, it was not possible to record their XRD diffractogram. Samples were not submitted to any thermal pre-treatment.

The total ionic conductivity of the ormolytes was determined by locating an electrolyte disk between two 10 mm diameter ion-blocking gold (Au) electrodes (Goodfellow, > 99.95%) to form a symmetrical cell. The Au/d-U(2000)$_n$LiBF$_4$/Au assembly was secured in a constant volume support [31] and installed in a Buchi TO51 tube oven with a type K thermocouple placed close to electrolyte disk to measure the sample temperature. Bulk conductivities of electrolyte samples were obtained during heating cycles using the complex plane impedance technique (Schlumberger Solartron 1250 frequency response analyzer and 1286 electrochemical interface) between 25 and 100 ºC and at approximately 7 ºC intervals.

Evaluation of the electrochemical stability window of electrolyte compositions was carried out within a dry argon-filled glovebox using a two-electrode cell configuration. The preparation of a 25µm diameter gold microelectrode surface by the conventional polishing routine was completed outside the glove box. The microelectrode was then washed with THF, dried with a hot-air blower and transferred to the interior of the glove box. Cell assembly was initiated by locating a freshly-cleaned lithium disk counter electrode (10 mm diameter, 1mm thick, Aldrich, 99.9% purity) on a stainless steel current collector. A thin-film sample of ormolyte was centered over the counter electrode and the cell assembly completed by locating and supporting the microelectrode in the centre of the electrolyte disk. The assembly was held together firmly with a clamp and electrical contacts were made to the Autolab PGSTAT-12 (Eco Chemie) used to record voltammograms at a scan rate of 100 mVs^{-1}. Measurements were conducted at room temperature within a Faraday cage located inside the measurement glovebox.

2.4. Construction and characterization of prototype ECDs

Solid-state ECDs were constructed using the four layer sandwich configuration shown in Scheme 1, which did not include an ion storage layer. The external layers of the ECDs were transparent conducting oxide films made of indium-doped zinc oxide (IZO) [32]. The active layers of the ECDs were an electrochromic film of tungsten oxide (WO_3) and an d-U(2000)$_n$LiBF$_4$ ormolyte film with n = 15, 10 and 8.

IZO films with a thickness 170 nm were deposited on two glass substrates by r. f. (13.56 MHz) magnetron sputtering using a ceramic oxide target In_2O_3:ZnO (92:8 wt%; 5 cm-diameter, Super Conductor Materials, Suffern, NY, U.S.A., purity of 99.99%). Sputtering was carried out at room temperature, with an argon flow of 20 cm^3 min^{-1} and an oxygen flow of 0.4 cm^3 min^{-1}. During sputtering the deposition pressure (argon and oxygen) was held constant at 0.15 Pa. The distance between the substrate and the target was 10 cm and the r. f. power was maintained at 100 W. WO_3 (Super Conductor Materials, purity of 99.99%) films with thickness of about 300 nm were deposited on the IZO-coated glass substrates by r. f. magnetron sputtering (Pfeiffer Classic 500). A small volume of the ormolyte sol was then spread onto the surface of the WO_3/IZO-coated glass plates. After a period of about 24 h, an IZO-coated glass plate was placed on top of the resulting ormolyte gel and the two plates were pressed together in such a way that the two coatings faced each other inside the assembled system (Scheme 1). In this manner a surface with an area of approximately 2.7 cm^2 was formed. Free space was left on each side for the electrical contacts. The entire assembly procedure described was carried out under atmospheric conditions.

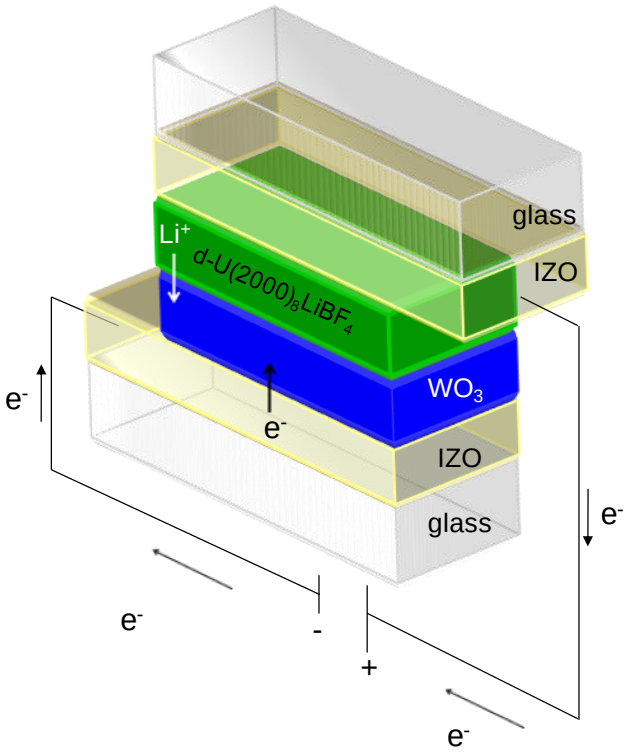

Scheme 1. Configuration of the prototype ECD studied (polarity for the coloration mode)

The application of a negative voltage of 1.5 V during 50 s to each glass/IZO/WO_3/d-U(2000)$_n$LiBF$_4$/IZO/glass ECD resulted in coloration from light yellow to deep blue. Electrons and Li^+ ions were transferred from the IZO and ormolyte films, respectively, to WO_3 which suffered simultaneous reduction and Li^+ insertion (Scheme 1). Bleaching (WO_3 oxidation and Li^+ desinsertion) from deep blue back to light yellow occurred upon reversing the applied voltage.

The optical transmittance of the ECDs was measured with a UV-VIS Spectronic Genexys 2PCC spectrophotometer and with a Shimadzu UV/VIS 3100PC double beam spectrophotometer.

Chronoamperometric (CA) tests of a glass/IZO/WO_3/d-U(2000)$_8$$LiBF_4$/IZO/glass ECD were performed using a potentiostat/galvanostat (Autolab model 100) by monitoring device current response as a function of time while the applied voltage was stepped between -4.0 V and +4.0 V with a delay time at each voltage of 50 s. The device was cycled 15 times (i.e., 1500 s) between the colored and bleached states. In the set-up used for measurements the electrolyte/WO_3/IZO substrate played the role of working electrode and the IZO layer acted as counter and reference electrodes. The cathodic and anodic charge densities were determined through integration of the CA curves during the coloring and bleaching processes.

The electrochromic memory was evaluated using a second glass/IZO/WO_3/d-U(2000)$_8$$LiBF_4$/IZO/glass ECD with the same active area, prepared under the same conditions and which had not been subject to any CA tests.

For the sake of clarity the ECDs used for CA measurements and for the electrochromic memory studies will be henceforth designated as ECD1 and ECD2, respectively.

3. RESULTS AND DISCUSSION

3.1. Structure and Morphology

Fig. 1(a) reproduces the XRD patterns of selected d-U(2000)$_n$$LiBF_4$ di-ureasils. As expected, the diffractogram of the non-doped sample (n = ∞) exhibits a broad band centered at about 21.0 º, caused by the ordering within the siliceous network. Two sharp and prominent peaks located at 18.9 and 23.1 º, associated with the presence of regions of crystalline, non-complexed short POE chains of the host d-U(2000) matrix [33] were also detected. The presence of both Bragg reflections in the diffractograms of the doped samples with n ≥ 15 confirms that in these materials the crystalline POE domains persist. In the case of d-U(2000)$_{15}$$LiBF_4$, the intensity of both diffracting peaks is significantly reduced. We also note that at n > 15 the relative intensity of the peaks at 18.9 and 23.1º is inverted (Fig. 1). At n = 8, although no trace of free crystalline POE remains, two new, very weak peaks, are visible at 38.5 and 44.9 º (Fig. 1(a)). In the XRD patterns of samples with n = 60, 20 and 15 these three peaks are also visible. Bragg peaks are also detected at about the same location in the XRD patterns of the d-U(600)$_n$$LiBF_4$ hybrids with n ≤ 10 investigated previously (Fig. 1(b)). As none of these peaks coincide with those of the XRD pattern of pure $LiBF_4$, they have been attributed to the formation of a new crystalline phase of unknown stoichiometry that exists in a minor proportion in the sample. These findings are in good agreement with the pseudo-equilibrium phase diagram of the $POE_n$$LiBF_4$ system proposed by Zahurak et al. [25]. These authors demonstrated that at n ≥ 4 free crystalline POE, amorphous material and the crystalline $POE_{3.5}$$LiBF_4$ complex coexist at room temperature. The absence of crystalline POE at room temperature in the sample with n = 8 strongly suggests that the eutectic temperature in the di-ureasil system is lower than in the case of the $POE_n$$LiBF_4$–based electrolytes (near 60 ºC [25]). This is an expected result since Chiodelli et al. [27] and Zahurak et al.

[25] used high molecular weight POE in their studies ($4x10^6$ and $5x10^6$ g mol^{-1}, respectively), whereas the POE of the d-U(2000) hybrid matrix has a significantly lower molecular weight (less than $2x10^3$ g mol^{-1}). Comparison of the XRD reflections characteristic of the $POE_{3.5}LiBF_4$ compound [25] with those observed in the d-U(2000)$_n$$LiBF_4$ ormolytes with $60 \geq n \geq 8$ at $29 < 2\theta$ (º) < 50 (Fig. 1) led us to conclude that the crystalline complex found in the POE-based system does not appear to be the same as that formed in the d-U(2000)-based hybrid medium.

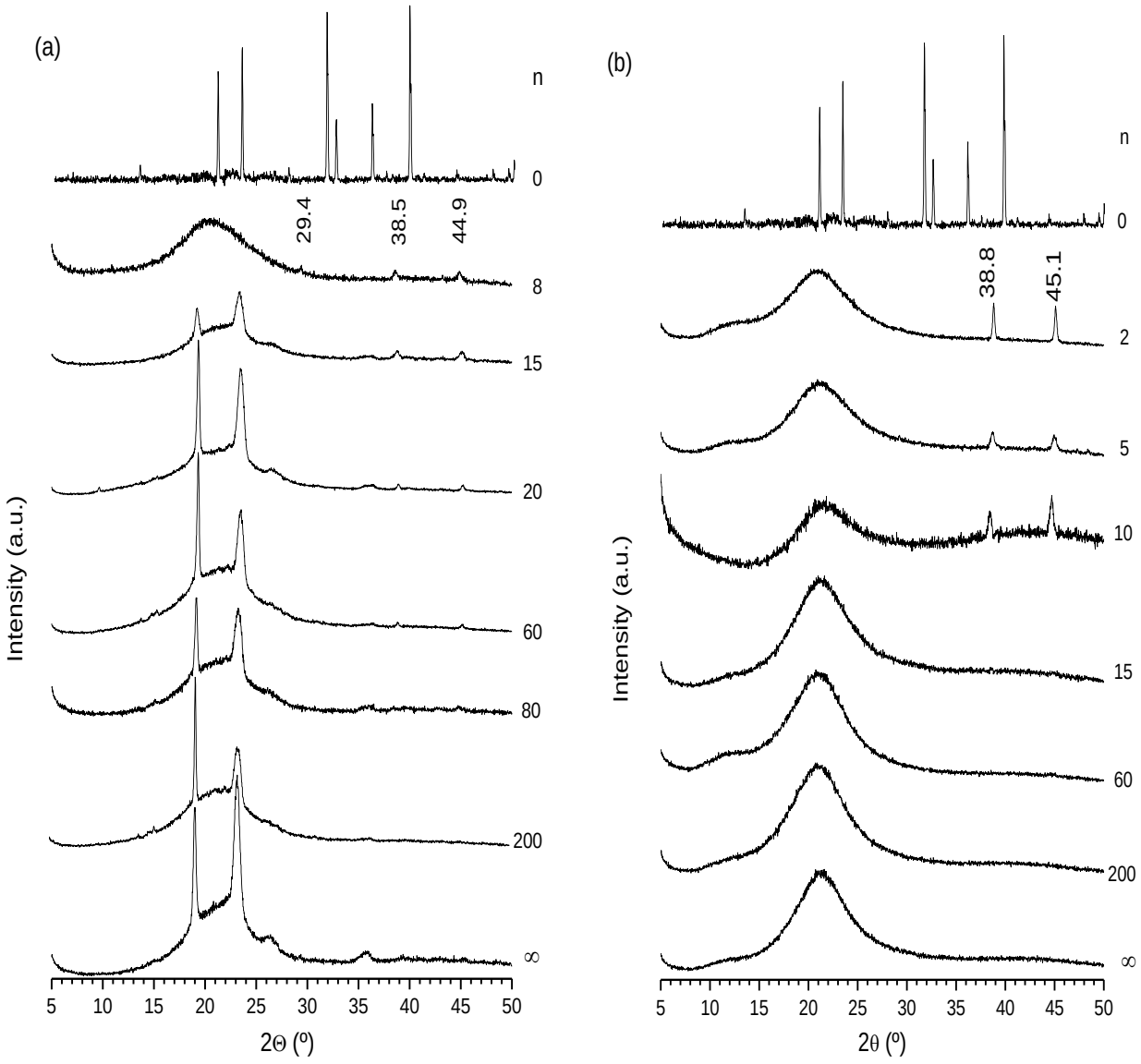

Figure. 1. XRD patterns of selected d-U(2000)$_n$$LiBF_4$ (a) and d-U(600)$_n$$LiBF_4$ (b) di-ureasils

The POM images of representative d-U(2000)$_n$$LiBF_4$ di-ureasil samples obtained between crossed polarizers (Fig. 2) confirm their anisotropic character. The birefringence observed suggests submicrometric anisotropy.

3.2. Thermal Behaviour

The DSC curves of d-U(2000)$_n$LiBF$_4$ samples in the 25-300 °C range are reproduced in Fig. 3. The thermogram of d-U(2000) displays two endothermic events below 50 ºC (Fig. 3), assigned to the fusion of free POE chains. Analysis of the DSC curves of the doped di-ureasils allows us to deduce that incorporation of LiBF$_4$ into the host d-U(2000) matrix produces semi-crystalline samples for n > 35 (Fig. 3). In the corresponding DSC curves the characteristic pair of thermal events attributed to the presence of crystalline, non-complexed POE regions is discerned.

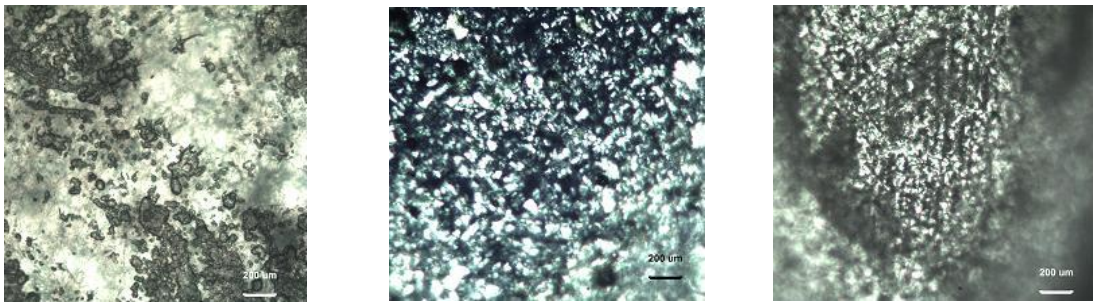

(A) (B) (C)

Figure 2. POM images of selected d-U(2000)$_n$LiBF$_4$ di-ureasils obtained between crossed polarizers: (a) n = ∞, (b) n =15; (c) n = 2.5

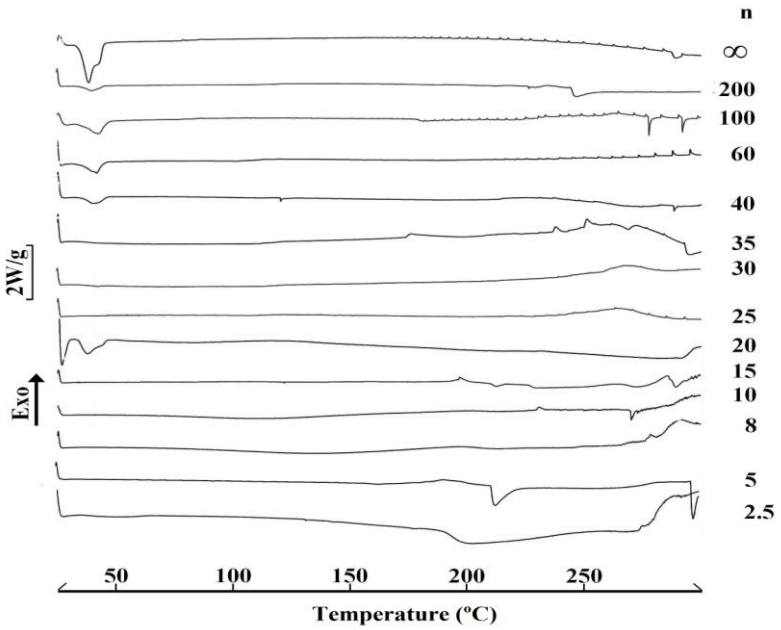

Figure 3. DSC curves of selected d-U(2000)$_n$LiBF$_4$ di-ureasils

At 35 ≥ n > 5 the materials become entirely amorphous, the sample with n = 20 being an exception, as both endotherms re-emerge in the DSC curve (Fig. 3).

In disagreement with the conclusions retrieved from XRD data, the DSC results suggest that in the di-ureasils with n = 35, 30, 25 and 15 no crystalline POE domains exist. Slow crystallization kinetics might explain this discrepancy, since the XRD and DSC measurements were performed in different periods of time. In the DSC curve of d-U(2000)$_5$LiBF$_4$ a sharp endothermic peak, centered at

approximately 215 ºC, is seen (Fig. 3). As the melting point of the pure salt is reported to lie between 293 and 300 °C, this event can only be ascribed to the fusion of a POE/$LiBF_4$

complex of unknown stoichiometry formed in the d-U(2000) medium. The broad, ill-resolved endothermic peak centered at about 200 ºC in the DSC curve of the salt-rich sample with n = 2.5 (Fig. 3) suggests that this crystalline complex exists at this composition.

It is useful to return to some relevant aspects of the pseudo-equilibrium phase diagrams proposed by Chiodelli et al. [27] and Zahurak et al. [25] for the POE_nLiBF_4 system. Both these studies propose the existence of a crystalline complex situated at $2 < n < 4$ and n = 3.5, respectively, that melts at about 150 ºC. This temperature is considerably lower (by 65 ºC) than the crystalline complex identified in the d-$U(2000)_nLiBF_4$ system. This result clearly indicates that the stoichiometries of the crystalline compounds formed in these two media are different. However, if the crystalline compound found in the POE_nLiBF_4 system were also formed in the di-ureasil medium, simply based on considerations of the average POE molecular weight, one would have expected to observe a lower melting temperature to be observed in the latter case. It should also be emphasized that the locations of the eutectic compositions reported ($6 < n < 8$ [27] and n = 16 [25]) do not coincide in the two pseudo-equilibrium phase diagrams proposed for the POE_nLiBF_4 system. If we rely on the XRD data, it seems plausible that in the case of the ormolyte system the eutectic is located at $15 > n > 8$.

Comparison of the DSC curves of the d-$U(2000)_nLiBF_4$ samples with those of the $LiCF_3SO_3$-[14], $LiClO_4$-[16] and LiTFSI [18]-doped d-U(2000) di-ureasils reveals that the thermal behavior of the $LiBF_4$-based system differs considerably from that of the three series of ormolytes indicated. These ormolytes are entirely amorphous in the same interval of salt concentration.

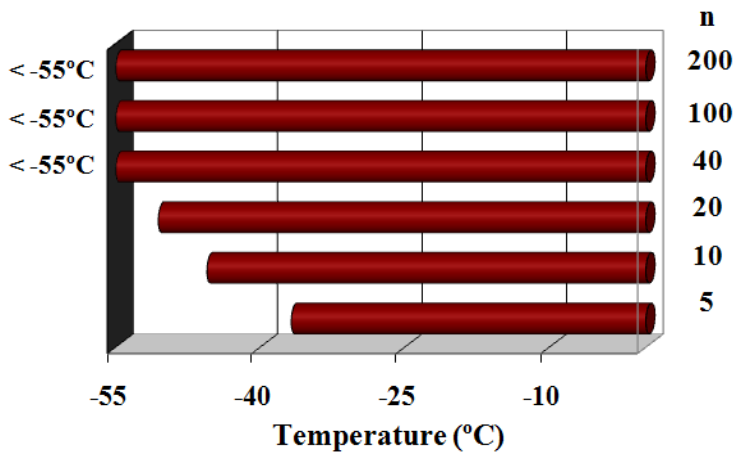

Figure 4. Composition dependence of the glass transition temperature of selected d-$U(2000)_nLiBF_4$ di-ureasils

Fig. 4 demonstrates that the glass transition temperature (T_g) of the doped di-ureasils with $n \geq 40$ is almost identical to the value reported for d-U(2000) (approximately -53 ◦C) [14]. In the high salt content range $n \leq 20$ the T_g of the d-$U(2000)_nLiBF_4$ samples increases markedly with salt concentration (Fig. 4). As the T_g of a polymer is defined as the temperature above which segmental motion begins, the trend observed confirms the existence of significant interactions between the Li^+ ions and the POE chains of the host hybrid matrix in the most concentrated d-$U(2000)_nLiBF_4$ sample. A similar

observation was previously reported for d-U(2000)-based di-ureasils doped with $LiCF_3SO_3$ [14] and $LiClO_4$ [16] in the same composition range and at $n \leq 35$ in the case of the d-U(2000)$_n$LiTFSI system [18].

Assuming that the initial mass loss observed for the samples with high salt content ($n \leq 10$) is exclusively associated with the release of adsorbed solvents (*e.g.*, water and/or ethanol), the DSC and TGA data are consistent with a minimum thermal stability of 225 ºC for samples with n = 10 and 5 (Figs. 3 and 5). In the case of the materials with lower salt content ($n \geq 20$) degradation starts at about 250 ºC (Fig. 5). In the ormolytes with d-U(2000)$_{100}$LiBF$_4$ and d-U(2000)$_{40}$LiBF$_4$ decomposition occurs in a single step (Fig. 5). The relatively low onset temperature of decomposition of the samples makes detection of free salt by thermal methods experimentally impossible (Fig. 3).

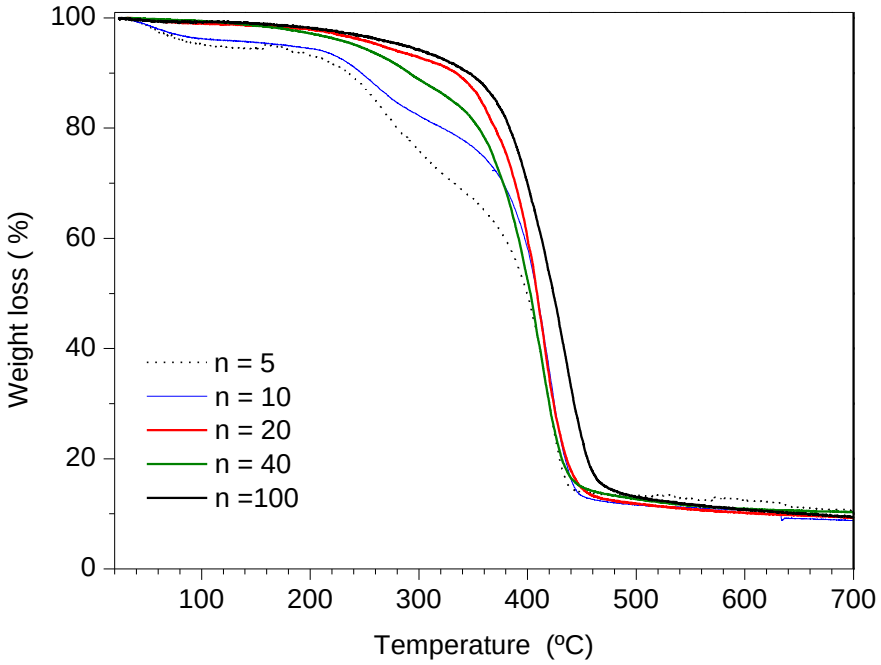

Figure 5. TGA curves of selected d-U(2000)$_n$LiBF$_4$ di-ureasils

These observations indicate that the thermal stability range of the d-U(2000)$_n$LiBF$_4$ ormolytes is similar to that observed with $LiClO_4$ [16]- and LiTFSI [18]-containing systems. The thermal data obtained in the present work confirm that $LiCF_3SO_3$ [14] is the guest salt that appears to have the most stabilizing influence on the d-U(2000) host network in a non-oxidizing atmosphere.

3.3. Ionic Conductivity

The Arrhenius plots of Fig. 6 and the conductivity isotherms reproduced in Fig. 7 demonstrate that that the most conducting di-ureasil composition, in the range of temperatures characterized, is the amorphous d-U(2000)$_{10}$LiBF$_4$ sample. At 22 ºC this sample exhibits 1.5×10^{-5} S cm^{-1} (Fig. 7), a value higher than those reported by Chiodelli et al. [27] and Zahurak et al. [25] for the POE$_n$LiBF$_4$ system.

This result was expected, as the POE-based electrolytes are typically poor conductors at ambient temperature due to the high proportion of crystalline material. This observation also confirms that the sol-gel strategy is beneficial in terms of reduction or even suppression of crystalline phases. At 97 ºC, d-U(2000)$_8$LiBF$_4$ is the hybrid electrolyte that supports the highest ionic conductivity (7.4×10^{-4} S cm^{-1}).

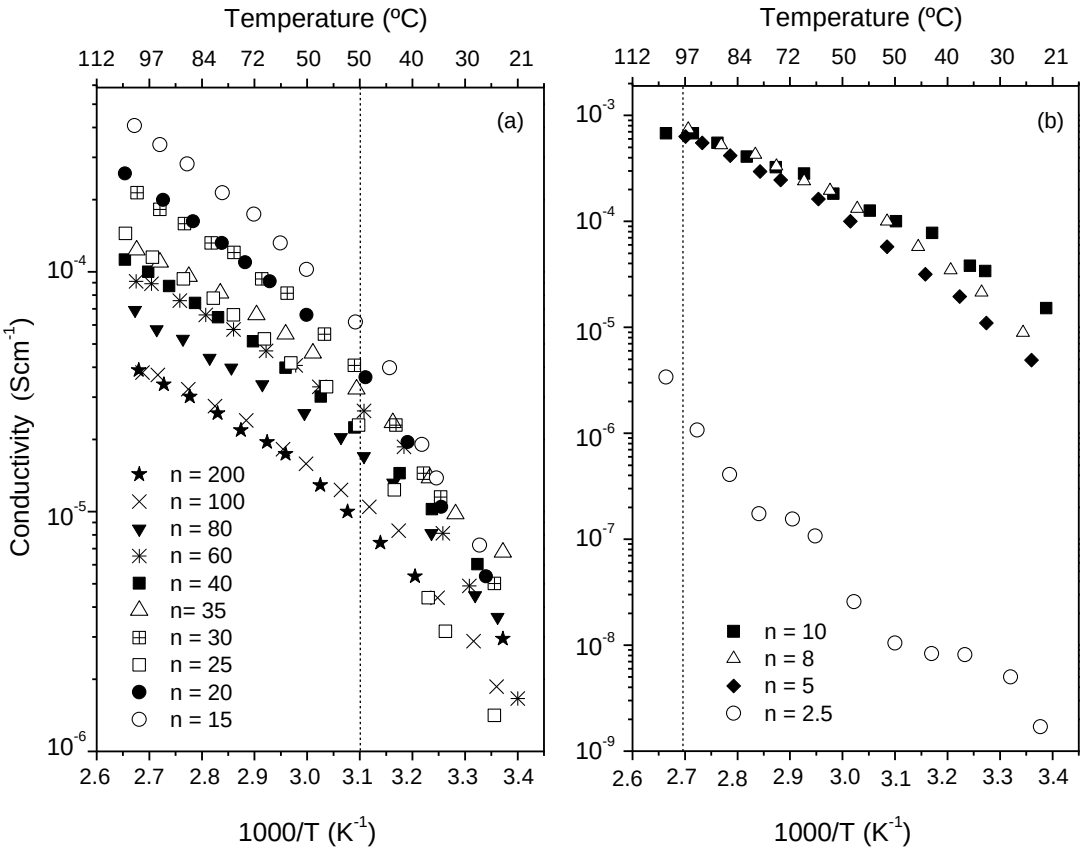

Figure 6. Arrhenius conductivity plots of the d-U(2000)$_n$LiBF$_4$ di-ureasils. The dotted lines drawn are intended as guides for the eyes.

Again, as expected, at higher temperatures the POE-containing electrolytes are better ionic conductors than the corresponding d-U(2000)-based ormolytes. At 100 ºC the POE$_{10}$LiBF$_4$ electrolyte exhibits a conductivity of about 10^{-3} S cm^{-1}.[27] Over the whole range of temperatures analyzed the lowest conductivity is detected in the material with n = 2.5 (1.7×10^{-9} S cm^{-1} at 23 ºC) (Fig. 6b). This behavior may also be associated with the presence of the crystalline POE/LiBF$_4$ complex of unknown stoichiometry and probably with the existence of free salt. Uncomplexed salt was not detected by DSC because, as explained above, the melting point of this salt is located at temperatures higher than the onset of thermal degradation. The high concentration of associated ionic species in this sample has been confirmed by the spectroscopic analysis discussed in the next section.

The behavior of the d-U(2000)$_n$LiBF$_4$ ormolytes with n ≥ 15 show two *quasi* linear regions, each exhibiting Arrhenius-type behavior (Fig. 6a). The inflection observed at about 50 º C (see dotted line in the graph) corresponds to the melting point of the POE chains of d- U(2000), as confirmed by the

DSC data (Fig. 3). In the salt-rich samples with 10 ≥ n > 2.5, a non-linear behavior, typical of amorphous materials, is evident (Fig. 6b).

Finally, it is worth comparing the conductivity data reported with the results published previously for the corresponding di-ureasil ormolytes doped with other guest lithium salts (Fig. 8). At 26 and 100 ºC the most conducting sample of the d-U(2000)$_n$LiCF$_3$SO$_3$ di-ureasil series was identified as n = 20 (5.8×x10^{-6} and 1.7×x10^{-4} Scm^{-1}, respectively) [14]. In the case of the d-U(2000)$_n$LiTFSI system, while the highest conductivity at 23 ºC was registered with the composition n = 35 (1.6×10^{-5} S cm^{-1}), at 95 ◦C the ormolyte that exhibited the highest conductivity is d-U(2000)$_{10}$LiTFSI (1.2×10^{-3} S cm^{-1}) [18].

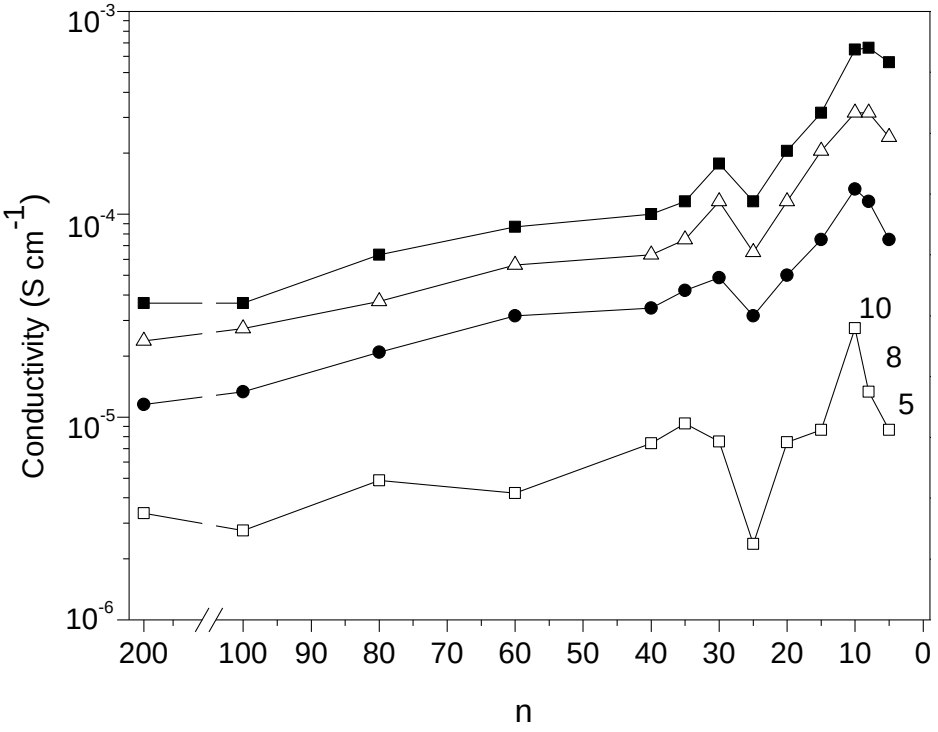

Figure 7. Conductivity isotherms of the d-U(2000)$_n$LiBF$_4$ di-ureasils

In the d-U(2000)$_n$LiClO$_4$ di-ureasils, the maximum conductivity at 22 ºC was detected in the sample d-U(2000)$_{30}$LiClO$_4$ (2.9×x10^{-5} S cm^{-1}) and at 100 ºC in the ormolyte with n = 5 (5.6×x10^{-4} S cm^{-1}) [16].

The choice of a salt to include in the formulation of an ormolyte for a lithium battery or an ECD is quite difficult. As LiClO$_4$ is often excluded on the basis of its explosive nature, LiBF$_4$ and LiTFSI are equally well-placed candidates as their ionic conductivity values are practically coincident (Fig. 8a).

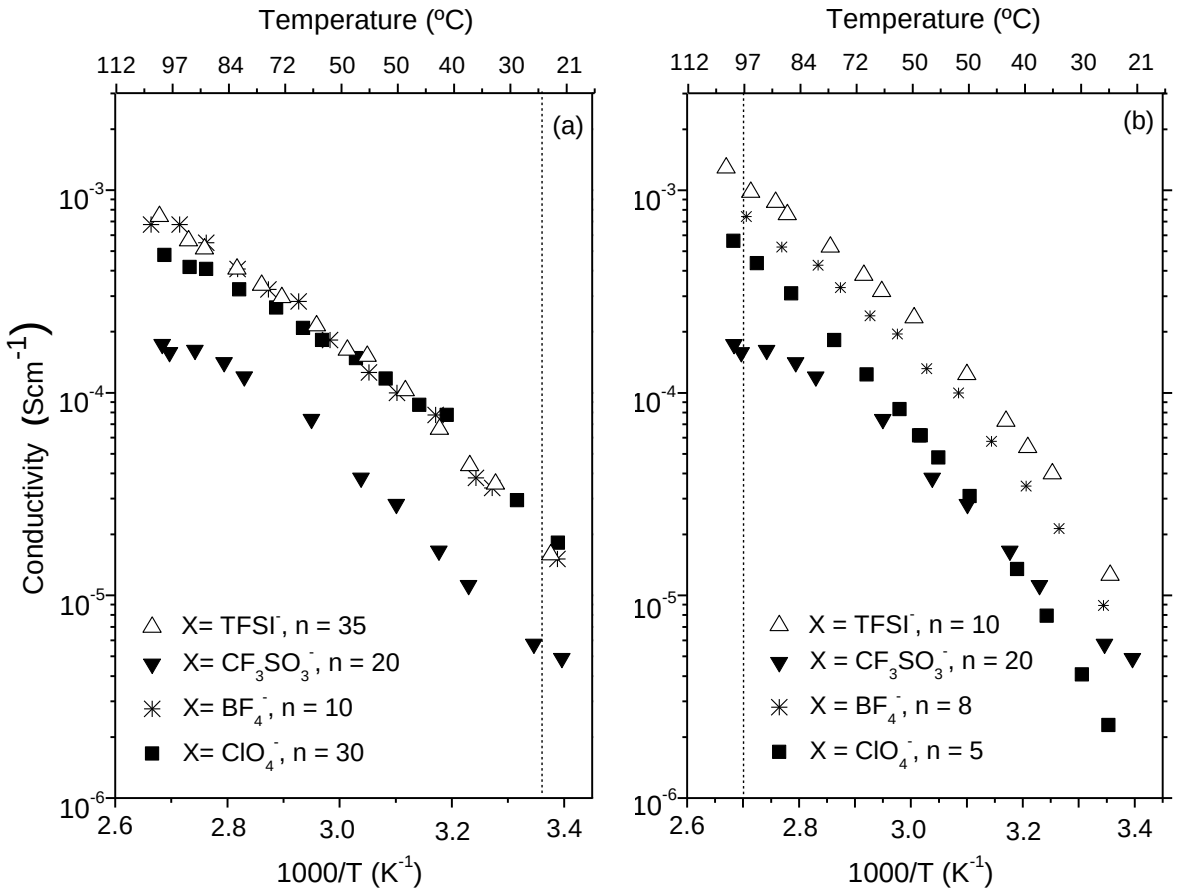

Figure. 8. Arrhenius conductivity plots of the conductivity maxima of d-U(2000)$_n$LiX di-ureasil systems at room (a) and high temperature (b). The lines drawn are intended as guides for the eyes.

3.4. Electrochemical Stability

The electrochemical stability of the d-U(2000)$_{15}$LiBF$_4$ di-ureasil material was determined by microelectrode cyclic voltammetry over the potential ranging from -3.0 to 6.5 V. Fig. 9a demonstrates that the overall redox stability of this ormolyte spans 5.5 V: while in the anodic region the sample is stable up to *ca.* 5.0 V *versus* Li/Li$^+$, in the cathodic region lithium deposition begins at about -0.5V *versus* Li/Li$^+$. Figs. 9b and 9c show that the electrochemical stability domain of this sample practically coincides with that reported previously for d-U(2000)$_{10}$LiTFSI and d-U(2000)$_{10}$LiClO$_4$ [16,18]. The data obtained lead us to suggest that the stability of the d-U(2000)$_{15}$LiBF$_4$ ormolyte is adequate for application in lithium primary and secondary cells.

3.5. Performance of prototype ECDs

A preliminary evaluation of the performance of the d-U(2000)$_n$LiBF$_4$ di-ureasil materials as electrolytes in all solid-state ECDs was performed. The devices were characterized by means of the following parameters: electrochromic contrast, optical density change, switching time, coloration efficiency and open circuit memory.

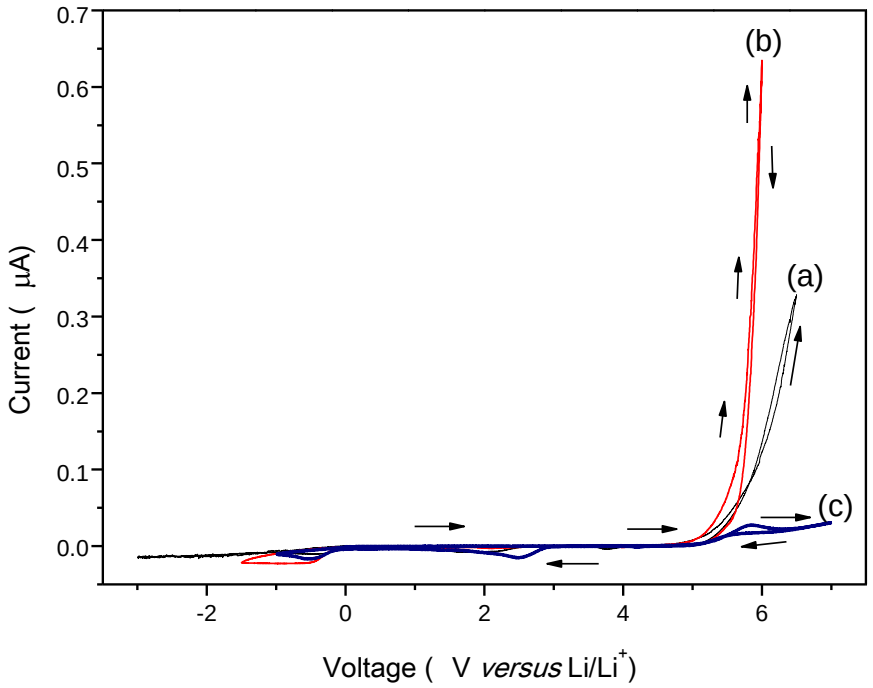

Figure 9. Room temperature cyclic voltamograms of the d-U(2000)$_{15}$LiBF$_4$ (a), d-U(2000)$_{15}$LiTFSI [18] (b) and d-U(2000)$_{10}$LiClO$_4$[16] (c) di-ureasils obtained with a 25 μm gold microelectrode as working electrode and lithium counter and reference electrodes (sweep rate = 100 mVs^{-1}).

The electrochromic contrast of an ECD may be described in terms of the percent transmittance change (Δ %T) at a particular wavelength or wavelength range. The transmission spectra recorded in the 380-760 nm range for the ECDs assembled incorporating the d-U(2000)$_n$LiBF$_4$ di-ureasil ormolytes with n = 8 and 10 – the samples which exhibit the highest ionic conductivity values of the series (Fig. 6(b) and Fig. 7), high transparency and excellent mechanical properties - are depicted in Figs. 10(a) and (b), respectively, in the as-deposited, bleached and colored states. The transmission spectra of the ECD incorporating the di-ureasil with n = 15, which exhibits a lower ionic conductivity than the two samples above (Fig. 6(a)), is shown is Fig. 10(c). All the spectra were recorded during the 1st coloring/bleaching cycle. The 1931 CIE photopic luminosity function, with a maximum at a wavelength of 555 nm (green), is also reproduced in Fig. 10 (dotted curve) (Note: The photopic vision is the vision of the human eye under normal lighting conditions during the day. It is responsible for color perception, being mediated by three biological pigments of the cones which sense light in three bands of color with maximum absorption values at 420 nm (blue), 534 nm (bluish-green) and 564 nm (yellowish-green)). All the spectra represented in Fig. 10 display a series of maxima and minima associated with interference originating from the multilayer nature of the device (Scheme 1). The

average transmittance in the visible region (400-700 nm) and the optical density change ($\Delta(OD) = -\log(T_{colored}/T_{bleached})$) exhibited by the three d-U(2000)$_n$LiBF$_4$–based ECDs are listed in Table 1. It is worth mentioning that the average transmittance of the as-deposited and bleached states are practically the same in the three cases, the value for all the bleached samples being higher than 66 % (Fig. 10 and Table 1). After coloration, ECD, which includes the d-U(2000)$_8$LiBF$_4$ ormolyte, presents an electrochromic contrast of *ca.* 18% and an $\Delta(OD)_{\lambda=555\ nm}$ of 0.13 (Table 1).

Table 1. Average spectral transmittance and optical density change in the visible region exhibited by ECDs incorporating d-U(2000)$_n$LiBF$_4$ di-ureasil ormolytes

	T (%)			$\Delta T_{bleached-colored}$	$\Delta(OD)$
n	as-deposited	colored	bleached	(%)	λ = 555 nm
15	72.2	58.7	71.5	12.8	0.09
10	68.8	56.7	66.9	10.2	0.07
8	73.9	54.1	72.1	18.0	0.13

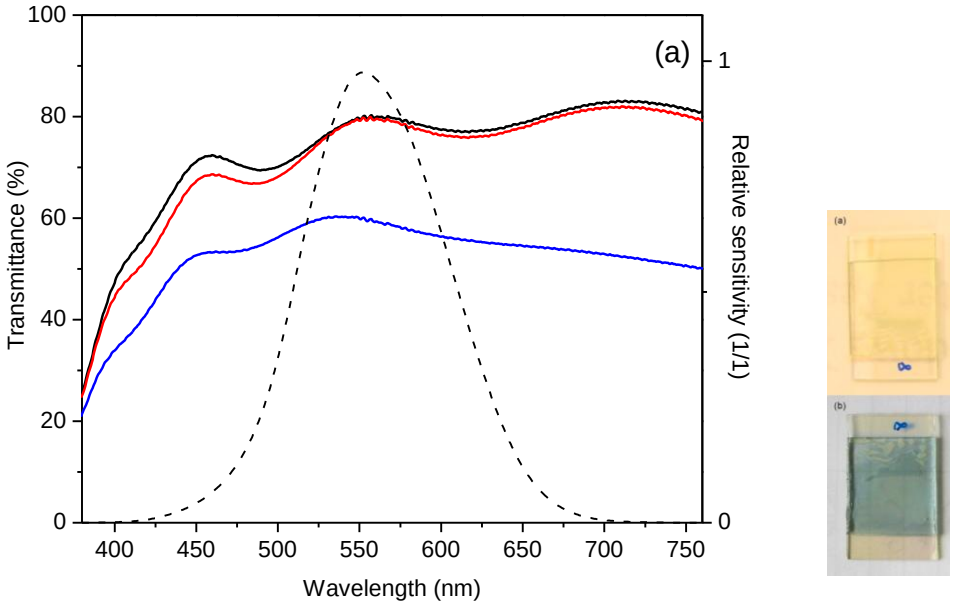

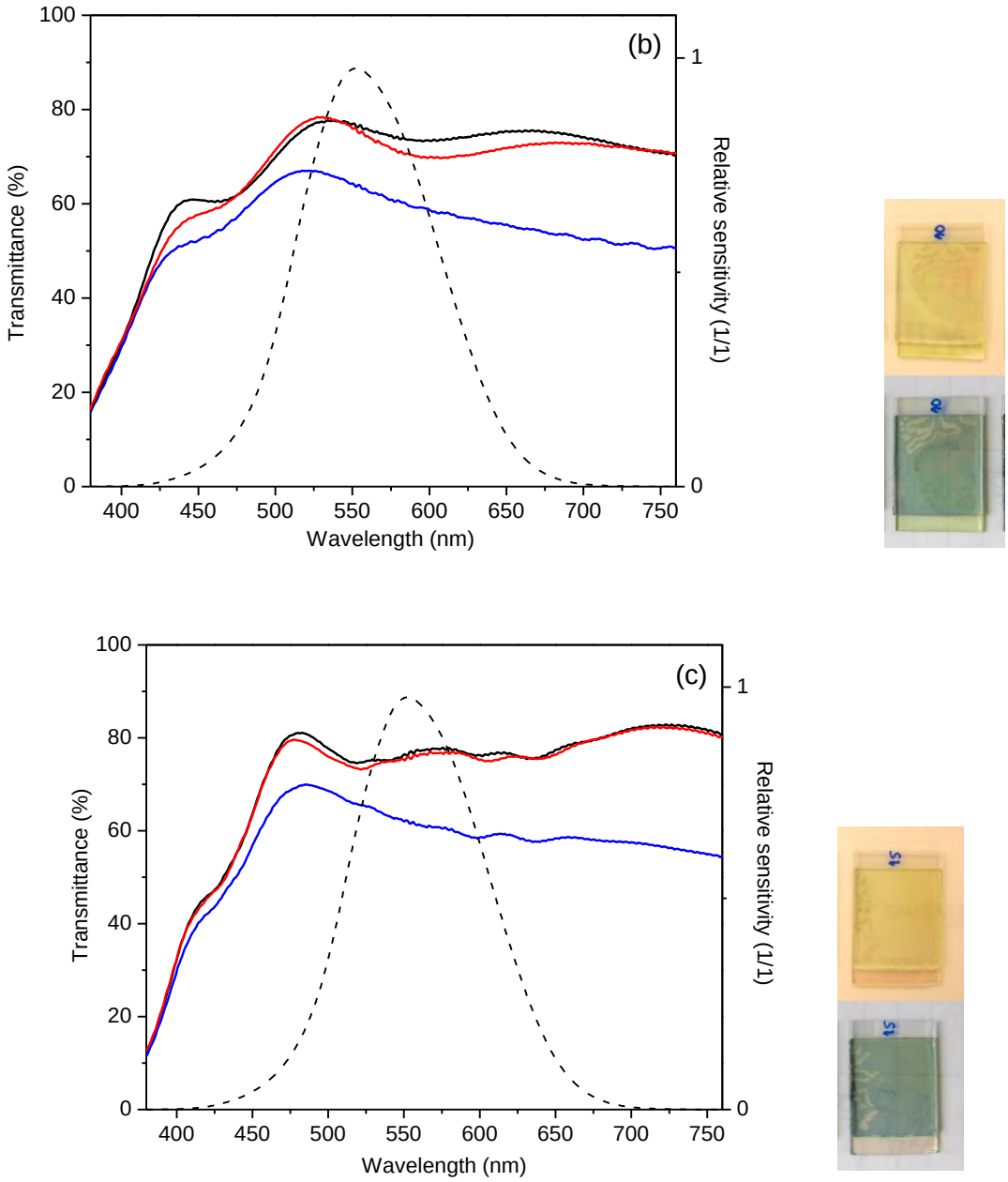

Figure 10. Optical transmittance (left axis) as a function of wavelength in the 380-760 nm region for the glass/IZO/WO_3/d-U(2000)$_n$LiBF_4/IZO/glass ECDs with n = 8 (a); n = 10 (b) and n = 15 (c), in the as-deposited (black line), bleached (red line) and colored (blue line) states in the 1st cycle.

The response time of the three ECDs studied, i.e., the time required for coloring/bleaching, was quite fast (approximately 50 s).

The wavelength dependence of the eye response is represented in dotted line (right axis). Photographs of the ECDs in the bleached and colored states are shown in the right hand side of the graphs.

The coloration efficiency of an ECD may be defined as the change in optical density per unit of inserted charge (CE = Δ(OD)/ΔQ). It is spectrally dependent. High CE values correspond to large

optical modulation at small charge insertion/desinsertion. The CE of the glass/IZO/WO_3/d-U(2000)$_8$LiBF$_4$/IZO/glass ECD2 was deduced from CA data (Fig. 11(a)). Fig. 11(b) allows concluding that the charge density decreases with the number of coloring/bleaching cycles. The charge insertion/desinsertion is not reversible, since the ratio of the cathodic to the anodic charges (Q_{in}/Q_{out}) is different from one.

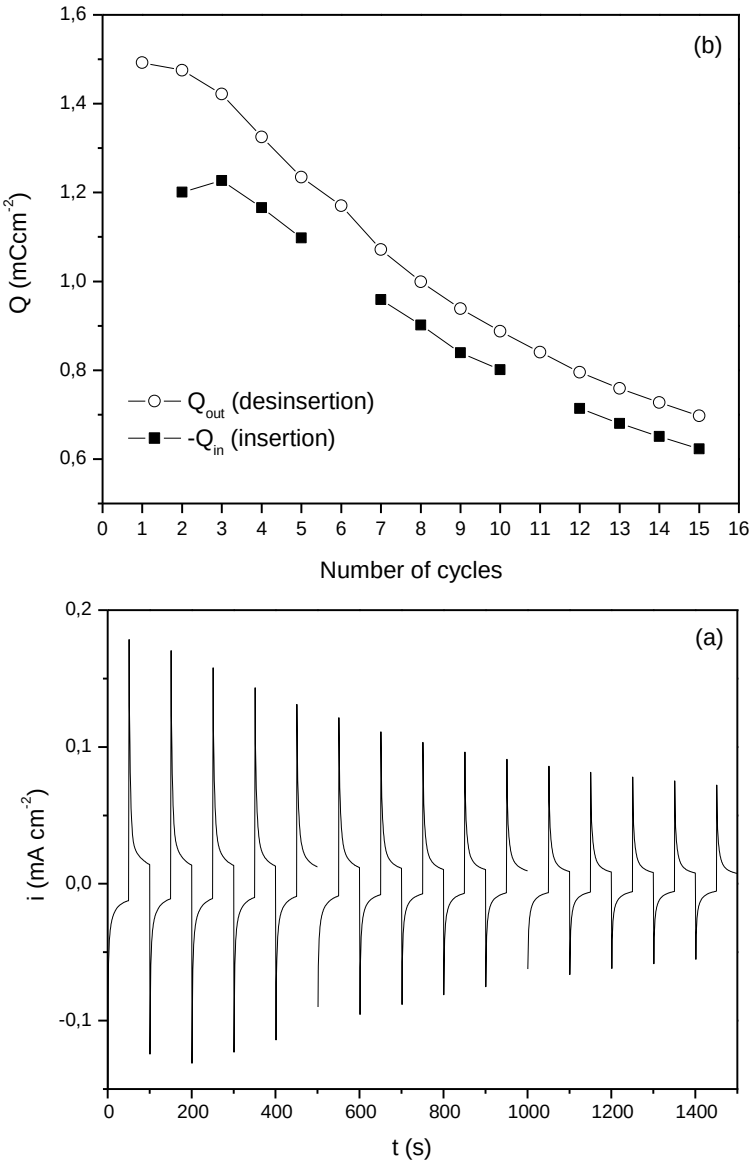

Figure 11. (a) Time dependence of the current density of the glass/IZO/WO_3/d-U(2000)$_8$LiBF$_4$/IZO/glass ECD1 with potential steps of -4 and + 4V at every 50 s (15 cycles). (b) Charge density of the glass/IZO/WO_3/d-U(2000)$_8$LiBF$_4$/IZO/glass ECD1 as a function of the number of cycles. The area of the device was assumed to be ideally 2.7 cm^2.

For the 3rd cycle a high CE value of 106 cm^{2}C^{-1} was estimated for a Δ(OD) of 0.13. Only thousands of CA cycles would allow us to draw further conclusions regarding the stability of this device.

The electrochromic memory was evaluated using the glass/IZO/WO_3/d-U(2000)$_8$LiBF$_4$/IZO/glass ECD2. Fig. 12 demonstrates that this device did not reach the as-deposited non-colored condition after being left for four months under open circuit conditions. A bluish hue was indeed still visible at eyesight.

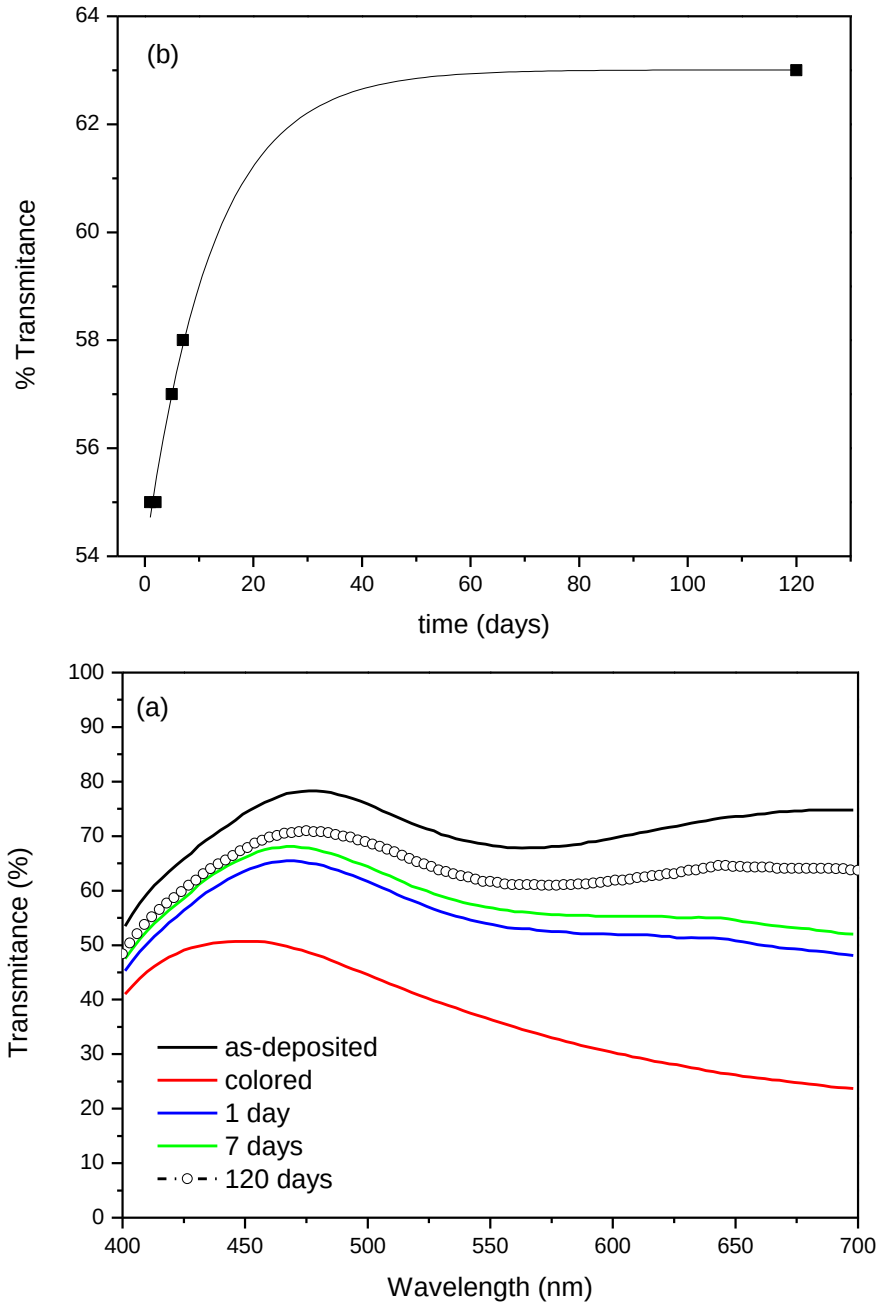

Figure 12. Time dependence of the transmission spectra (a) and average transmittance (b) in the visible region of the glass/IZO/WO_3/d-U(2000)$_8$LiBF$_4$/IZO/glass ECD2 only cycled once. The curve drawn is (b) is just a guide for the eyes.

The preliminary results obtained for the prototype ECDs fabricated with d-U(2000)$_n$LiBF$_4$ di-ureasils are quite encouraging. However, various fundamental aspects remain to be examined in future studies. For instance, the reason for the variation of the Δ(OD) with ormolyte composition is not clear. At λ = 620 nm the Δ(OD) values calculated (not shown) are slightly lower than those reported for the d-U(2000)-based di-ureasil ormolyte systems doped with LiTFSI [18] and $LiClO_4$ [34]. Problems, such as the presence of air and/or defects in the electrolyte films produced during sealing (see photographs in Fig.10), might account for the fact that the di-ureasil sample that displays the highest room temperature conductivity (i.e., d-U(2000)$_{10}$LiBF$_4$) and which should in principle supply more ions, is not the one that leads to the best results. The optimization of the ECD assembly procedure is therefore required for the improvement of the performance of the devices. Moisture control during device construction should also be considered in future work. Another compulsory aspect to take into account in future tests is the inclusion of a counter-electrode layer with high ion-storage capacity. The inclusion of this component in the ECDs will provide a sufficient number of ions for deeper coloration of the WO_3 layer at lower voltage, consequently endowing the devices with enhanced stability and enhanced cyclability.

4. CONCLUSIONS

In the present study, we have investigated di-urea cross-linked POE/siloxane hybrids doped with a wide range of LiBF$_4$ concentration ($\infty > n \geq 2.5$). In the presence of LiBF$_4$ and at $n \geq 15$ a proportion of the POE chains of the host d-U(2000) matrix exists in the crystalline state. A crystalline POE/LiBF$_4$ complex of unknown stoichiometry is formed in samples with $60 \geq n \geq 2.5$. In the most concentrated sample studied free salt is probably present. The results of the conductivity measurements have shown that the LiBF$_4$-doped di-ureasil hybrid electrolytes may be viable alternatives to the LiTFSI-based polymer electrolytes. In addition, the thermal and electrochemical stability of the LiBF$_4$-based di-ureasils are sufficient to justify further studies to develop attractive electrolyte components for practical devices. The preliminary tests carried out with ECDs including the d-U(2000)$_n$LiBF$_4$ di-ureasils as ion conducting active layers allow to foresee the application of these materials in "smart windows" and other ECD-based devices, thus justifying further studies.

ACKNOWLEDGMENTS

The financial support provided by Fundação para a Ciência e a Tecnologia (FCT) (contracts POCI/QUI/59856/2004 and POCTI/SFA/3/686) is gratefully acknowledged. P. C. Barbosa and M. Fernandes thank FCT for grants (contracts SFRH/BD/22707/2005 and SFRH/BD/38530/2007, respectively) and travel funds (P. C. Barbosa).

References

1. F. M. Gray, Solid Polymer Electrolytes: Fundamentals and Technological Applications, VCH Publishers, New York (1991)
2. M. Armand, J. M. Chabagno, M. Duclot, Extended Abstracts Second International Conference on Solid Electrolytes, St Andrews, Scotland (1978)
3. J.-M. Tarascon, M. Armand, *Nature* 414 (2001) 359
4. P. Gomez-Romero, C. Sanchez (Eds.), Functional Hybrid Materials, Wiley-VCH, New York, (2003)
5. C. J. Brinker, G. W. Scherer, Sol-Gel Science, The Physics and Chemistry of Sol-Gel Processing, Academic Press, CA (1990)
6. D. Ravaine, A. Seminel, Y. Charbouillot, M. Vincens, *J. Non-Cryst. Solids* 82 (1986) 210
7. M. Popall, M. Andrei, J. Kappel, J. Kron, K. Olma, B. Olsowski, *Electrochim. Acta* 43 (1998) 1155
8. P. Judeinstein, J. Titman, M. Stamm, H. Schmidt, *Chem. Mater*. 6 (1994) 127
9. K. Dahmouche, M. Atik, N. C. Mello, T. J. Bonagamba, H. Panepucci, M. A. Aegerter, P. Judeinstein, *J. Sol–Gel Sci. Technol*. 8 (1997) 711
10. V. de Zea Bermudez, L. Alcácer, J. L. Acosta, E. Morales, *Solid State Ionics* 116 (1999) 197
11. C. Wang, Y. Wei, G. R. Ferment, W. Li, T. Li, *Mater. Lett*. 39 (1999) 206
12. J. R. MacCallum, S. Seth, *Eur. Polym. J*. 36 (2000) 2337
13. K. Nishio, T. Tsuchiya, *Sol. Energy Mater. Sol. Cells* 68 (2001) 295
14. S. C. Nunes,V. de Zea Bermudez, D. Ostrovskii, M. M. Silva, S. Barros, M. J. Smith, R. A. Sá Ferreira, L. D. Carlos, J. Rocha, E. Morales, *J. Electrochem. Soc*. 152 (2005) A429
15. S. C. Nunes, V. de Zea Bermudez, M. M. Silva, M. J. Smith, L. D. Carlos, R. A. Sá Ferreira, J. Rocha, *J. Solid State Electrochem*. 10 (2006) 203
16. M. M. Silva, S. C. Nunes, P. C. Barbosa, A. Evans, V. de Zea Bermudez, M. J. Smith, D. Ostrovskii, *Electrochim. Acta* 52 (2006) 1542
17. S. C. Nunes, V. de Zea Bermudez, D. Ostrovskii, P. B. Tavares, P. C. Barbosa, M. M. Silva, M. J. Smith, *Electrochim. Acta* 53 (2007) 1466
18. P. C. Barbosa, M. M. Silva, M. J. Smith, A. Gonçalves, E. Fortunato, S. C. Nunes, V. de Zea Bermudez, *Electrochim. Acta* 54 (2009) 1002
19. S. M. Gomes Correia, V. de Zea Bermudez, M. M. Silva, S. Barros, R. A. Sá Ferreira, L. D. Carlos, A. P. Passos de Almeida, M. J. Smith, *Electrochim. Acta* 47 (2002) 2421
20. C. Sanchez, B. Julián, P. Belleville, M. Popall, *J. Mater. Chem*. 15 (2005) 3559
21. M. Armand, C. Poinsignon, J.-Y. Sanchez, V. de Zea Bermudez, U.S. Patent, 5283310, 1993.
22. P. C. Barbosa, L. Rodrigues, M. M. Silva, M.J. Smith, A. Gonçalves, E. Fortunato, *J. Mater. Chem.*, 20 (2010) 723
23. S. S. Zhang, K. Xu, T. R. Jow, *J. Electrochem. Soc*. 149 (2002) A586
24. S. S. Zhang, K. Xu, T. R. Jow, *Electrochem. Comm*. 4 (2002) 928
25. S. S. Zhang, K. Xu, T. R. Jow, *J. Solid State Electrochem*. 7 (2003) 147
26. S. M. Zahurak, M. L. Kaplan, E. A. Rietman, D. W. Murphy, R. J. Cava, *Macromolecules* 21 (1988) 654
27. M. M. Silva, S. C. Barros, M. J. Smith, J. R. MacCallum, *Electrochim. Acta* 49 (2004) 1887
28. G. Chiodelli, P. Ferloni, A. Magistris, M. Sanesi, *Solid State Ionics* 28-30 (1988) 1009
29. M. B. Armand, J. M. Chabagno, M. J. Duclot, *Polyethers as Solid Electrolytes*, in: P. Vashita, J. N. Mundy, G. K. Shenoy (Eds.), Fast Ion Transport in Solids, *Elsevier, Amsterdam*, 1979, pp.131-136.
30. M. Fernandes, P. C. Barbosa, M. M. Silva, M. J. Smith, V. de Zea Bermudez, Materials Chemistry and Physics, accepted
31. C. J. R. Silva, M. J. Smith, *Electrochim. Acta*, 40 (1995) 2389
32. E. Fortunato, L. Pereira, P. Barquinha, I. Ferreira, R. Prabakaran, G. Goncalves, A. Goncalves, R. Martins, R. *Philos. Mag*. 89 (2009) 2741
33. L. D. Carlos, V. de Zea Bermudez, R. A. Sá Ferreira, L. Marques, M. Assunção, *Chem. Mater*., 11 (1999) 581

34. P.C. Barbosa, M. M. Silva, M. J. Smith, A. Gonçalves, E. Fortunato, *Electrochim. Acta* 2007, 52, 2938